Original Research Article

Assessment of the Validity of Carbon Ion Irradiation for C6 Gliomas in Rats

Dose-Response:
An International Journal
Vol. 23(2): 1–12

DOI: 10.1177/15593258251327505
journals.sagepub.com/home/dos
Sage

Yufeng Li[1,2,3], Lei Ta[4], QingFeng Wu[5], Hongyu Zhang[1,2,3], Yuan Xu[1,2,3], Lu Gan[5], and Jianli Liu[1,3]

Abstract

Purpose: Application of energy-spectrum computed tomography (CT) to assess specific efficacy of and response to carbon ion radiotherapy (CIRT) of C6 gliomas in rats.
Methods: After establishing C6 glioma rat models, 3 tumor-bearing rats were randomly selected as controls. The remaining were divided into 0 Gy, 1 Gy, and 2 Gy groups for CIRT. Energy-spectrum CT scans were performed, and brain tissues were collected for histopathology and western blot Test. Survival rates in each group were compared.
Results: The results demonstrated that tumors in the 1 Gy and 2 Gy groups decreased at different rates up to 14 days post-CIRT ($P < 0.05$). Furthermore, compared to pre-CIRT measurements, the energy-spectrum parameters gradually increased in the 0 Gy group, while they decreased in the 2 Gy group. Post-CIRT, the Ki-67 proliferation index and the expression levels of vascu-larassociated proteins in tumor tissues were significantly reduced in the 1 and 2 Gy groups. Additionally, the survival times of tumor-bearing rats were prolonged after CIRT.
Conclusions: CIRT effectively restricts tumor cell growth and proliferation, leading to improved survival rates in rats with C6 gliomas. The use of energy-spectrum CT with immunohistochemistry for quantitative detection can actively support the effectiveness of carbon ion radiotherapy in inhibiting tumor proliferation.

Keywords

radiobiological effects, carbon ion irradiation, gliomas, energy-spectrum CT

Received: 15 July 2024; accepted: 18 February 2025

Introduction

Glioblastomas (GBMs) account for approximately 48.6% of all malignant cranial tumors. Over the past decade, there has been a gradual increase in the average annual incidence of GBMs in adolescents and children.[1,2] Currently, the primary treatment for GBM involves surgery combined with radiotherapy or chemotherapy. However, since GBMs grow invasively with unclear boundaries, the extent of surgical resection and any remaining tumor tissue directly impact the patient's prognosis.[3,4] Moreover, although radiotherapy can partially control local tumor growth and improve overall survival (OS) in patients with GBM, their prognoses are still poor.[5,6] Unfortunately, GBM is resistant to radiation, requiring a higher dose, which can cause necrosis in the normal tissues surrounding the target. Additionally, the highly infiltrative

[1] Department of Radiology, Lanzhou University Second Hospital, Lanzhou, China
[2] Second Clinical School, Lanzhou University, Lanzhou, China
[3] Key Laboratory of Medical Imaging of Gansu Province, Lanzhou University Second Hospital, Lanzhou, China
[4] Ningbo Medical Center LiHuiLi Hospital, Ningbo, China
[5] Institute of Modern Physics, Chinese Academy of Sciences, Lanzhou, Gansu, China

Corresponding Authors:
Jianli Liu, Department of Radiology, Lanzhou University Second Hospital, No.82, Cuiyingmen, Linxia Road Street, Lanzhou, Gansu 730000, China.
Email: liujl_1219@163.com

Lu Gan, Institute of Modern Physics, Chinese Academy of Sciences, 1 Yanxia Road, Lanzhou, Gansu 730000, China.
Email: ganl@impcas.ac.cn

growth pattern of GBM makes precise targeting challenging, and early tumor recurrence oc-curs in the majority of patients (90%).[7] Therefore, it is crucial to explore safe and effective radiotherapy methods.

Carbon ion beams have an inverted depth dose distribution, known as the Bragg peak, enabling the precise treatment of tumors by controlling and adjusting the peak area of the radiation dose, detecting the irradiation range in real time, and reducing the radiation dose to organs at risk. This diminishes the probability of post-radiotherapy complications.[6,8] Specifically, carbon ion beams are rays with high linear energy transfer (LET) that cause complex, difficult-to-repair DNA damage and stimulate apoptosis in tumor cells.[9,10] In vitro studies in different glioma cell lines have shown that carbon ion irradiation (CIR) has a higher cell-killing effect, is less dependent on the oxygen enhancement ratio than X-rays, and can overcome the radiation resistance of tumor cells.[11,12] Furthermore, recent clinical trial data suggest that carbon ion radiotherapy (CIRT) combined with chemotherapy is beneficial for GBM treatment.[13,14] However, the use of CIRT to treat gliomas is still in the clinical research phase, with minimal clinical data available or in development. Moreover, it is difficult to acquire pathology specimens for clinical assessment. To address these issues, one of the best options is to establish a stable and effective animal model to study the specific efficacy of CIRT in the treatment of GBM.

C6 gliomas in rats show similar behaviour and pathology to human cerebral glioblastoma.[15] Magnetic resonance imaging (MRI) is mostly used for the clinical detection of brain tumors and the assessment of their efficacy.[16,17] With the development of imaging technology, energy-spectrum CT has gradually become a popular option in re-search. The benefits of CT imaging include enabling base material separation and quantitative analysis, obtaining the effective atomic number, iodine concentration (IC), and water concentration of each pixel point, and identifying the material composition and functional state. These provide great clinical value in the differential diagnoses of diseases, prognoses, and tumor grading and typing.[18,19]

In this study, we established a rat C6 glioma model, administered different doses of CIR, and used energy-spectrum CT scanning for post-CIR dynamic detection. We also included histopathological staining and molecular biotechnology to explore the inhibitory effect of different doses of CIR on the growth and proliferation of rat C6 gliomas and to provide a theoretical basis for its application in clinical treatment.

Methods and Materials

Ethics

The research duration is from March 2022 to March 2023. The project received approval from the Ethics Committee of Lanzhou University Second Hospital and was conducted according to the ARRIVE guidelines (D2019-041). We obtained experimental rats from the Lanzhou Institute of Veterinary Medicine, Chinese Academy of Agricultural Sciences, with ananimal license number SCXK (Gan 2020-0002). We selected 85 healthy, male Sprague–Dawley rats with a clean grade, weighing 220 ± 20 g, and exhibiting good mental status and growth.

Tumor Model Preparation

To begin the experiment, all rats were anesthetised by intraperitoneal injection of 2% sodium pentobarbital (2 mL/kg) and secured in the prone position on a stereotaxic apparatus. We made a midline incision in the scalp, exposing the sagittal and coronal sutures. Next, we drilled 4-mm holes to the right of the sagittal suture and 1-mm holes anterior to the coronal suture using an electric drill. Using a microsyringe, we slowly inserted a needle to a depth of 5 mm from the skull into the reserve cell space. We then injected 10 μL of C6 glioma cell suspension in the logarithmic growth phase at a rate of 1 μL/min (containing 1.0 × 106 cells/μL). After completing the injection, we left the needle in place for 5 min before slowly withdrawing it. We then closed the cranial holes using bone wax and sutured and disinfected the skin.

CIR

Approximately 14 days after implanting the C6 cells, we performed energy-spectrum CT enhancement scans to observe tumor formation. We randomly selected 6 tumor-bearing rats as pre-CIR pathological controls, and the remaining rats were irradiated with varying doses of the carbon ion beam from a medical heavy ion gas pedal unit at the Wuwei Heavy Ion Cancer Treatment Center, Gansu Province, China. The rats were anaesthetised, and their heads were positioned in the optimal area for localised irradiation with the carbon ion beam. The carbon ion beam had an elicitation energy of 260 MeV/u and a LET of 50 keV/μm. We set the irradiation doses to 0 Gy (control group), 1 Gy, and 2 Gy. After irradiation, we housed the rats and recorded their survival time.

Image Data Acquisition

Energy-spectrum CT enhancement scans were performed 1 day pre-CIR and at 7, 14, and 21 days after CIR. The rats were anaesthetised, and an indwelling needle was used to puncture the tail vein. An infusion cannula was then used to connect the syringe to the intravenous indwelling needle. Each rat was fixed in the prone position on the scanning machine for head-first scanning. A dose of 2.5 mL/kg of the contrast agent 320 iodixanol (320 mgI/mL) was injected at a rate of 0.2 mL/s. We used a GSI scanning mode with a scanning frame rotation speed of 0.5 s/r and a detector width of 2 cm. The scan field of view was set to small head, and the display field of view was set to 9 cm in standard reconstruction mode. We used the adaptive statistical iterative reconstruction-V 30%, scanning

matrix of 512 × 512, X-ray voltage of 80 kVp with instantaneous switching, a tube current of 630 mA, a layer thickness of 0.652 mm, and a delay time of 20 s. After completing the scanning, each rat was placed in a 37°C incubator for anaesthesia recovery.

Image Analysis

The raw CT scan images were transferred to a GE AW4.7 workstation (GE Healthcare, Chicago, IL, USA) for data measurement and analysis using the GSI viewer analysis software (GE Healthcare, Chicago, IL, USA). The axial map of the tumor at the maximum diameter level under 70 keV conditions was selected for measuring energy spectral data and tumor volume. Two regions of interest with a diameter of 0.5 mm were placed in the solid area of the tumor (R1) and the contralateral normal brain tissue area (R2). Necrotic cystic lesions, large blood vessels, and ventricles were avoided whenever possible. Each region was measured 3 times, and the average value was used for statistical analysis. The single-energy CT values at 40-140 keV, the best single-energy CT value ($CT_{70\ keV}$), and the iodine concentration (IC) were recorded, and the slope of the energy spectrum curve "K" was calculated. The energy spectrum curve was plotted using the formula: $K_{(40\text{-}70\ keV)} = CT(40\text{-}70\ keV)/(70\text{-}40)$. The largest trans-verse (a) and long (b) diameters of the tumor were measured 3 times, and the volume of the tumor (mm3) was calculated using the formula: $(mm3) = (a \times b) \times 4\pi/3$; $\pi = 3.14$.

Histopathological Staining

Three tumor-bearing rats were selected before CIR, and 3 rats were selected from each group on days 7, 14, and 21 after CIR for histopathological staining. The rats were anaesthetised, and cardiac perfusion was performed. Whole brain tissues were then taken and preserved in 4% paraformaldehyde after labelling with the animal number and collection time. The samples were layered in paraffin and frozen in 5-μm sections after 24 h. Haematoxylin–eosin (HE) staining and Ki-67 immunohistochemistry staining were carried out. The stained sections were scanned and analysed using a panoramic light microscope (3DHISTECH, Hungary).

Preparation of Tissue Lysates and Western Blotting

Three tumor-bearing rats were selected pre-CIR, and an additional 3 rats per group were chosen on days 7 and 14 post-CIR. These rats were anesthetized with a 2% pentobarbital sodium injection and then euthanized via cervical dislocation. Tumor samples were collected and proteins were prepared for Western blot analysis. Briefly, 10 μg of extracted protein from each sample was separated on 12% polyacrylamide gels and then transferred onto PVDF membranes. To block non-specific binding, the membranes were incubated with TBS-T buffer containing 2% skim milk. Membranes were then incubated with primary antibody at 4°C overnight, followed by dilution with anti-mouse or rabbit IgG H anti-mouse or rabbit IgG HPR antibody. Finally, the membranes were exposed to Immobilin Western Chemilumi-nescent HRP substrate (Merck, KGaA., Darmstadt, Germany), and chemiluminescent signals were detected using an AI680 Gel imaging system. Western blotting experiments were performed 1-3 times per sample.

Statistics Analysis

All statistical analyses were performed using SPSS 25.0 (IBM Corp., Armonk, NY, USA) and GraphPad Prism 9.0.0 (GraphPad Software, Boston, MA, USA). All results were expressed as the mean (± standard deviation). The ANOVA test was chosen as the appropriate statistical method for comparing the study outcomes among the study groups. The Kaplan–Meier method was used for the survival analysis of each rat group, excluding rats that underwent tissue collection. The Pearson correlation test was used to analyze the correlation between the energy spectrum parameters and the Ki-67 value-added index. The level of significance was set at $P < 0.05$.

Results

Tumorigenic Detection and Rat Survival Analysis

A tumourigenic assay was performed 14 days after C6 glioma cell implantation. Seven rats had no significant nodules in the right basal ganglia region on the energy-spectrum CT-enhanced scans, and we considered that the modelling had failed. The remaining 78 rats were included in the follow-up study. Six tumor-bearing rats were randomly selected as pre-irradiation molecular and pathological controls, and 72 were randomly divided into 3 groups (24 each) for CIR.

Survival analysis revealed that the median survival time for rats in the 0 Gy group was 22 days (95% confidence interval [CI], 18.61-25.40 days), while for the 1 Gy group it was 30 days (95% CI, 24.16-35.84 days), and for the 2 Gy group it was 33 days (95% CI, 18.40-47.61 days). The survival time of the 1 Gy and 2 Gy groups showed a statistically significant difference when compared to the 0 Gy group ($P < 0.05$) (Figure 1).

Morphological Characteristics

CT imaging showed nodule-like enhancement, with part of the enhancement exhibiting a ring-shaped pattern (see Figure 2). There was no statistically significant difference in the tumor volumes in each group before CIR (Table 1). However, the tumor volume gradually increased in all 3 groups 7 days after CIR, with the 0 Gy group showing the most significant differences ($P < 0.01$). The tumor volume of the 0 Gy group increased over time, and the central liquefied necrotic area showed significant garland-like enhancement. In this group,

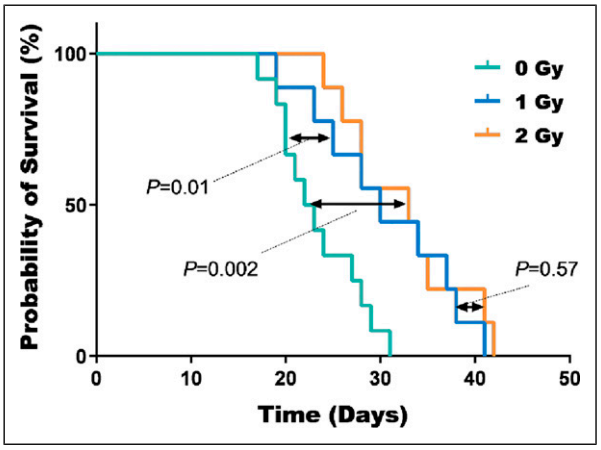

Figure 1. Plots of Kaplan–Meier survival curves as a function of post-implantation days for 3 different groups (0 Gy, n = 12; 1 Gy, n = 9; 2 Gy, n = 9). The rats were observed daily until 42 days post-implantation. Both the 1 Gy and 2 Gy groups survived longer than the 0 Gy group ($P < 0.01$ and $P < 0.002$, respectively).

the tumor encroachment was evident, with the right lateral ventricle becoming flattened, the longitudinal fissure of the brain deviating to the left, and compression observed on the left side of the brain. Fourteen days after CIR, the tumor volume of the 1 Gy and 2 Gy groups was significantly reduced, showing a statistical difference from that of the 0 Gy group ($P < 0.001$). The tumors' solid areas were reduced, and liquefied areas were observed around them. Six rats in the 1 Gy group and 5 in the 2 Gy group survived until 21 days after CIR. Four rats in the 1 Gy group and 3 in the 2 Gy group showed further reduction in volume and multiple liquefactions in the peritumoural area. The difference in tumor volume be-tween the 2 groups was not statistically significant ($P < 0.05$).

Multiparametric Quantification of the Energy Spectrum CT

We analyzed the differences in the energy spectra between the tumors and the normal brain tissue in the 2 Gy group (Figure 3A–C). Compared with the normal tissue, the tumor was mixed hypointense and enhanced significantly on scans, with $CT_{70\ keV}$, IC, and $K_{(40\text{-}70\ keV)}$ significantly higher. IC in the solid tumor area was significantly reduced at 7 and 14 days post-CIR. $CT_{70\ keV}$ and $K_{(40\text{-}70\ keV)}$ were significantly reduced at 14 days post-CIR, statistically significant differences were observed compared to pre-CIR ($P < 0.05$). At 21 days post-CIR, energy spectral parameters in the tumor areas increased to varying degrees, possibly associated with tumor recurrence.

We further analysed the differences in energy spectral parameters between the groups at different time points (Figure 3D–F), and the differences between the groups pre-CIR were not statistically significant. Compared with pre-CIR, IC was significantly reduced in the 2 Gy group at 7 days post-CIR, and $CT_{70\ keV}$, IC, and $K_{(40\text{-}70\ keV)}$ were differently reduced in the 1 Gy and 2 Gy groups at 14 days post-CIR. Moreover, compared with 0 Gy group, post-CIR (1 and 2 Gy) each energy spectrum parameter was decreased to different degrees, and the difference was statistically significant (Table 1).

Histological Evaluation and Immunohistochemical Staining

The tumor cells in the 0 Gy group exhibited obvious infiltrative growth. The central necrotic area was enlarged and surrounded by multiple hyperplastic blood vessels and pseudopalisading tumor cells. At 7 days after CIR, obvious necrotic areas were observed in the centre of the tumor in the 1 Gy and 2 Gy groups. Nuclear consolidation, fragmentation, and lysis were also observed at the junction of the solid and necrotic areas. The volume of tumor cells decreased and vacuolisation changes were observed. Furthermore, the infiltration of tumor cells into the periphery was reduced.

At 14 days after CIR in the 1 Gy and 2 Gy groups, the tumor cells were sparsely arranged and multiple liquefied areas were found in both the center and periphery of the tumor. There was no apparent peritumoural infiltration. After 21 days of CIR, the tumor had significantly decreased in size and was partially replaced by a large liquefied area. Associated with this, there was peripheral vascular hyperplasia and infiltration of tightly arranged spindle-shaped tumor cells, suggesting the possibility of tumor recurrence or progression (Figure 4).

The positive expression of Ki-67, a proliferating cell nuclear antigen, reflects the tumor's proliferative capacity. Figure 5 displays the results of Ki-67 immunohistochemical staining. The Ki-67 proliferation indices were as follows: 28.67% pre-CIR, 35.33% in the 0 Gy control group at 7 days after CIR, 29% in the 1 Gy group at 7 days after CIR, 22.67% in the 2 Gy group at 7 days after CIR, 42.67% in the 0 Gy group at 14 days after CIR, 19% in the 1 Gy group at 14 days after CIR, 17.67% in the 2 Gy group at 14 days after CIR, 23% in the 1 Gy group at 21 days after CIR, and 21% in the 2 Gy group at 21 days after CIR. The Ki-67 value-added index of tumor tissues significantly decreased after CIR.

Correlation Analysis of Energy Spectrum Parameters with Ki-67 Value-Added Indices

Within the observation time, $CT_{70\ keV}$, IC and $K_{(40\text{-}70\ keV)}$ were significantly increased in the 0 Gy group, and the Ki-67 value-added index was significantly increased. Conversely, $CT_{70\ keV}$, IC and $K_{(40\text{-}70\ keV)}$ decreased to varying degrees post-CIR (1 and 2 Gy), and Ki-67 proliferative index also gradually decreased, except for 21 days post-CIR. Pearson's correlation test showed strong positive correlations between $CT_{70\ keV}$, IC and $K_{(40\text{-}70\ keV)}$ and the Ki-67 value-added index, respectively (Figure 6).

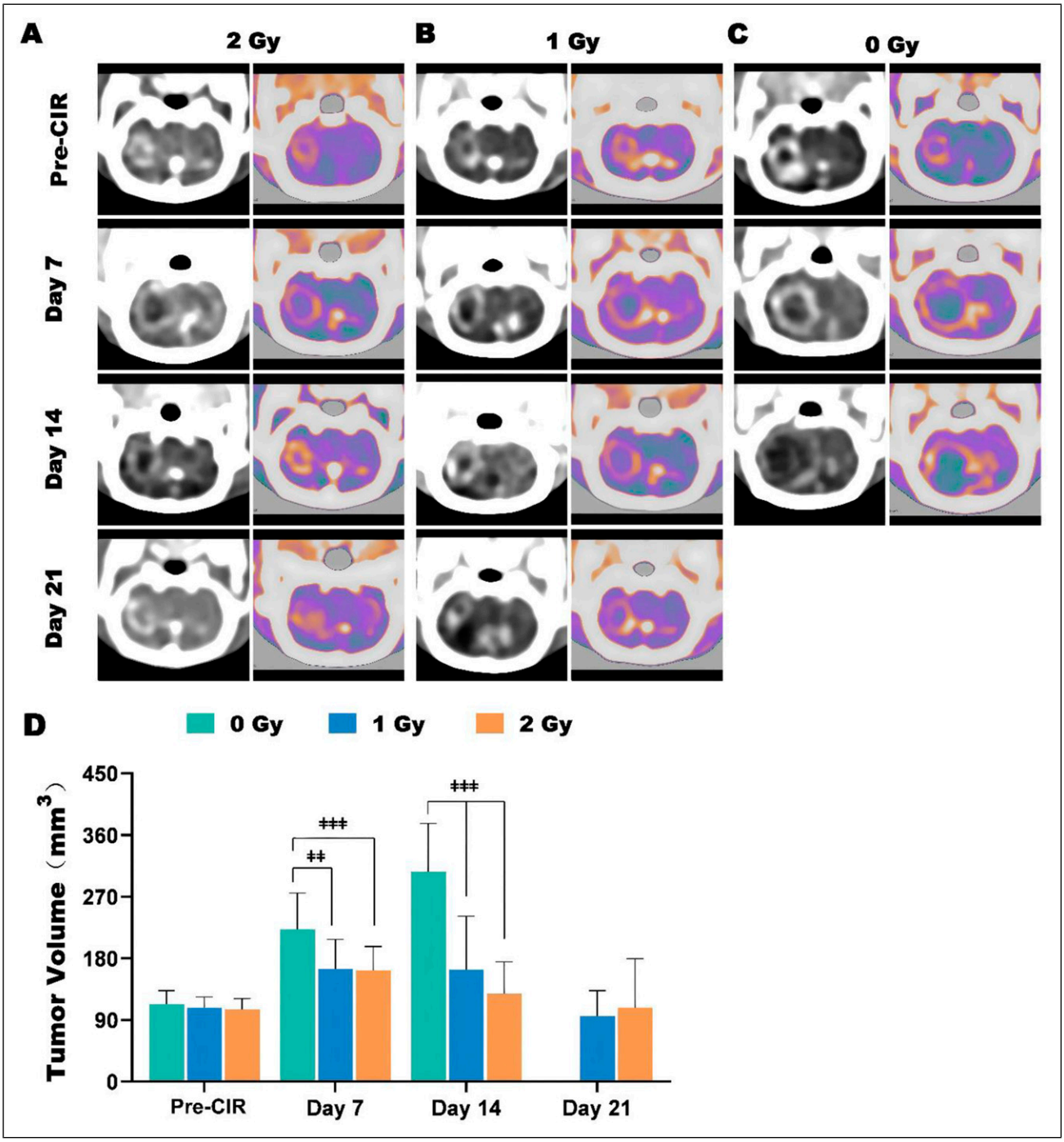

Figure 2. (A-C) Energetic CT characterisation images of 3 groups of rats (2 rats per group) obtained at different time points (pre-CIR and at 7, 14, and 21 days post-CIR). On day 7 post-CIR, the tumor volumes of the 3 groups increased significantly. (D) Tumor volume was measured using energy spectrum CT enhancement scanning with a single energy map at 70 keV at different time points. Statistical significance of differences compared with pre-irradiation: $^{ǂ}P < 0.05$, $^{ǂǂ}P < 0.01$, $^{ǂǂǂ}P < 0.001$.

Vascular-Related Protein Western Blot Test Results

As shown in Figure 7, the expression levels of vascular-related proteins were significantly up-regulated in the 0 Gy group. Seven days post-CIR, the expression of vascular-related proteins in the 2 Gy group was significantly down-regulated compared to the 0 Gy group during the same period. Additionally, the expression of VEGFA and VEGFR-2 in the 1 Gy group was significantly down-regulated ($P < 0.05$). At 14 days post-CIR, the expression levels of vascular-related proteins in tumor tissues were significantly down-regulated in the 1 Gy and 2 Gy groups. These

Table 1. Changes in Tumor Volume and Energy Spectrum Parameters in Pre-and Post-carbon Ion Irradiation.

Parameter	Dose	Pre-CIR	Day 7	Day 14	Day21
Tumor volume (cm^3)	0 G y	113.13 ± 19.58	222.53 ± 52.81	305.99 ± 70.70	__ __
	1 G y	108.06 ± 15.58	164.62 ± 43.01*	163.59 ± 77.85*	95.63 ± 37.19
	2 G y	105.01 ± 15.98	162.25 ± 34.78*	127.97 ± 46.95*	108.29 ± 71.23
$CT_{70\ keV}$ (HU)	0 G y	93.64 ± 8.76	121.02 ± 17.66	142.48 ± 11.87	__ __
	1 G y	95.42 ± 4.24	101.71 ± 7.49*	89.53 ± 8.50*	96.72 ± 14.07
	2 G y	96.46 ± 8.14	97.04 ± 8.42*	88.36 ± 4.84*	94.42 ± 8.08
IC (100ug/cm3)	0 G y	22.25 ± 6.83	27.87 ± 9.24	38.96 ± 11.21	__ __
	1 G y	22.45 ± 6.94	21.84 ± 3.47*	16.45 ± 4.70*	19.80 ± 8.81
	2 G y	25.17 ± 3.99	19.92 ± 3.41*	15.14 ± 3.14*	21.28 ± 10.71
$K_{(40\text{-}70\ keV)}$	0 G y	3.99 ± 1.38	5.32 ± 1.75	7.37 ± 2.09	__ __
	1 G y	3.71 ± 1.25	3.82 ± 1.20*	3.16 ± 1.28*	5.86 ± 2.88
	2 G y	4.08 ± 1.04	3.60 ± 1.50*	2.94 ± 1.17*	3.76 ± 0.52

Values are given as mean ± SD.
*vs 0 Gy group, $P < 0.05$, not marked = not significant.

differences were statistically significant compared to the 0 Gy group ($P < 0.001$).

Discussion

CIRT is now being used to treat malignant and re-current tumors, including prostate cancer, pancreatic cancer, non-small-cell lung cancer, and breast cancer.[20-23] However, CIRT for glioma is still in the clinical research stage.[24-26] In a study by Lautenschlaeger et al, the effects of CIRT and photon reirradiation therapy on OS in patients with recurrent GBM were compared and analysed. The results suggest that CIRT is a safe and feasible treatment option for patients with recurrent GBM.[27] However, due to the limited sample size and challenges in obtaining tumor samples for pathological analysis, further investigation is needed to fully understand the efficacy of CIRT.

Rat C6 gliomas share similarities with human glioblastomas in terms of biology and pathology, making them a useful model for studying changes before and after GBM CIRT.[28] In our study, we successfully established 57 rat C6 glioma models and recorded the survival status and time of rats before and after exposure to different doses of carbon ions. The results showed that carbon ion irradiation significantly improved the quality of life and survival time of the rats, with notable effects observed in the 2 Gy group. However, considering the differences between animal models and human patients in disease resistance, it is crucial to gather more clinical information to determine if different species with GBM can benefit from CIRT.

Carbon ion beams are high LET rays with higher relative biological effectiveness.[9,29] Research has shown that both primary GBM and recurrent GBM patients can tolerate CIRT well with minimal toxic reactions.[30,31] However, the specific effects of CIRT on local GBM control have not been extensively reported. Research shows that CIR causes glioma cells to enlarge through vacuolation and mitochondrial swelling, leading to cell senescence and death. This indicates that carbon ion beams can effectively eliminate tumor cells by promoting aging and death.[32,33] In this study, significant necrosis appeared within the tumor 7 days post-CIR at 1 and 2 Gy groups, and although the tumor volume increased, HE staining showed a large number of necrotic tumor cells within the tumor. 14 days post-CIR, tumors showed significant shrinkage with surrounding liquefaction. HE staining revealed a substantial decrease and thinning of tumor cells, some of which developed vacuoles and merged into larger cells. Ki-67 immunohistochemistry indicated a reduced tumor proliferation index. This indicates that carbon ion beams have a potent cell-killing effect and effectively inhibit the proliferation of C6 glioma cells. At 21 days post-CIR, fewer surviving rats were observed. Some tumors regressed, but others grew, signaling recurrence and progression typical of glioblastoma, and highlighting the need for retreatment.

Quantitative energy-spectral CT parameters can detect microstructural changes within malignant gliomas, provide important information about the extent of tumor proliferation and invasion, and help identify glioma recurrence and treatment-related changes.[34] In addition, 65-70 keV single-energy CT images have the best contrast signal to noise ratio, and the slopes of the energy spectral curves under 40-70 keV single-energy conditions have high clinical value.[15,35,36] In this study, $CT_{70\ keV}$, $K_{(40\text{-}70\ keV)}$ and IC were recorded, and dynamic quantitative detection of the response to glioma treatment in rats after CIR was analysed. The results showed that $CT_{70\ keV}$, $K_{(40\text{-}70\ keV)}$, and IC tended to increase over time in the 0 Gy group. Additionally, compared with the pre-CIR group, although the tumor volume of the 1 Gy and 2 Gy groups increased 7 days post-irradiation, the IC of both groups and the $K_{(40\text{-}70\ keV)}$ of the 2 Gy group decreased. Combining these results with the HE staining, which showed a large amount of tumor cell necrosis during the same period, we believe that IC and $K_{(40\text{-}70\ keV)}$ can respond to the inhibitory

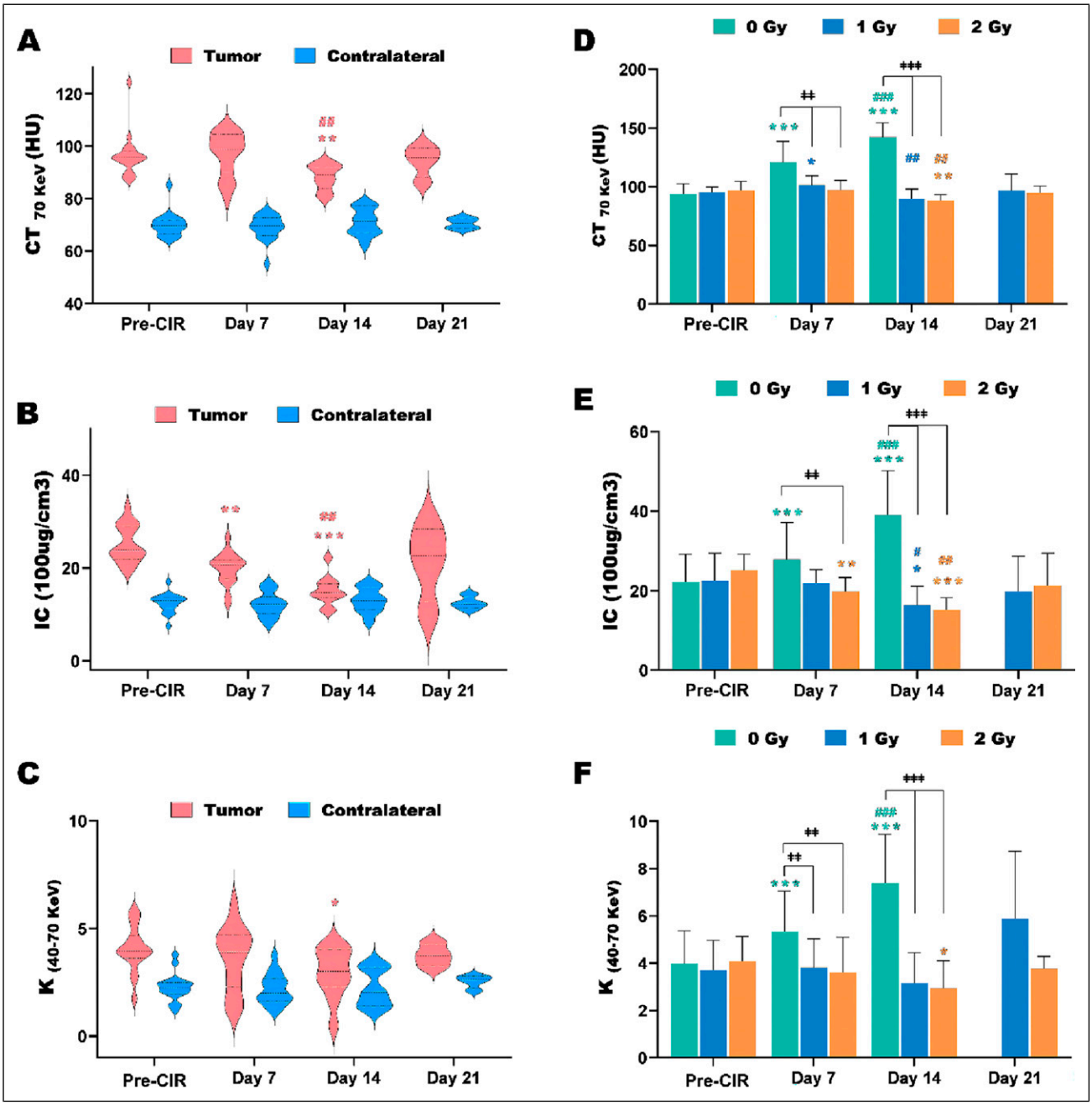

Figure 3. (A-C) Quantitative analysis of energy spectrum CT multiparameters at different time points pre- and post-CIR in the tumor area and contralateral normal tissue area (n = 18) of rats in the 2 Gy group. (D-F) Quantitative multiparameter analysis of energy spectral CT of the solid tumor area at multiple time points pre-and post-CIR at different doses. The differences were statistically significant compared with the 0 Gy group: ǂ$P < 0.05$, ǂǂ$P < 0.01$, ǂǂǂ$P < 0.001$; and compared with those pre-CIR: $P < 0.05$, *$P < 0.01$, ***$P < 0.001$; and compared with those 7 days post-CIR: #$P < 0.05$, ##$P < 0.01$, ###$P < 0.001$.

effect of carbon ion irradiation on tumor cell proliferation earlier.

At 14 days post-CIR, $CT_{70\ keV}$, $K_{(40\text{-}70\ keV)}$ and IC were significantly reduced in the irradiation groups, and the difference was statistically significant compared with 0 Gy group. Compared with the pre-CIR or 7 days post-CIR, the $CT_{70\ keV}$ and IC of the irradiation groups were significantly reduced, and the differences were statistically significant, suggesting that $CT_{70\ keV}$ and IC can react to the dynamic change process of rat glioma before and after carbon ion irradiation with greater sensitivity.

At 21 days post-CIR, each energy-spectrum parameter of the irradiated groups in-creased to different degrees, with $K_{(40\text{-}70\ keV)}$ being the most prominent. The results of both HE staining and

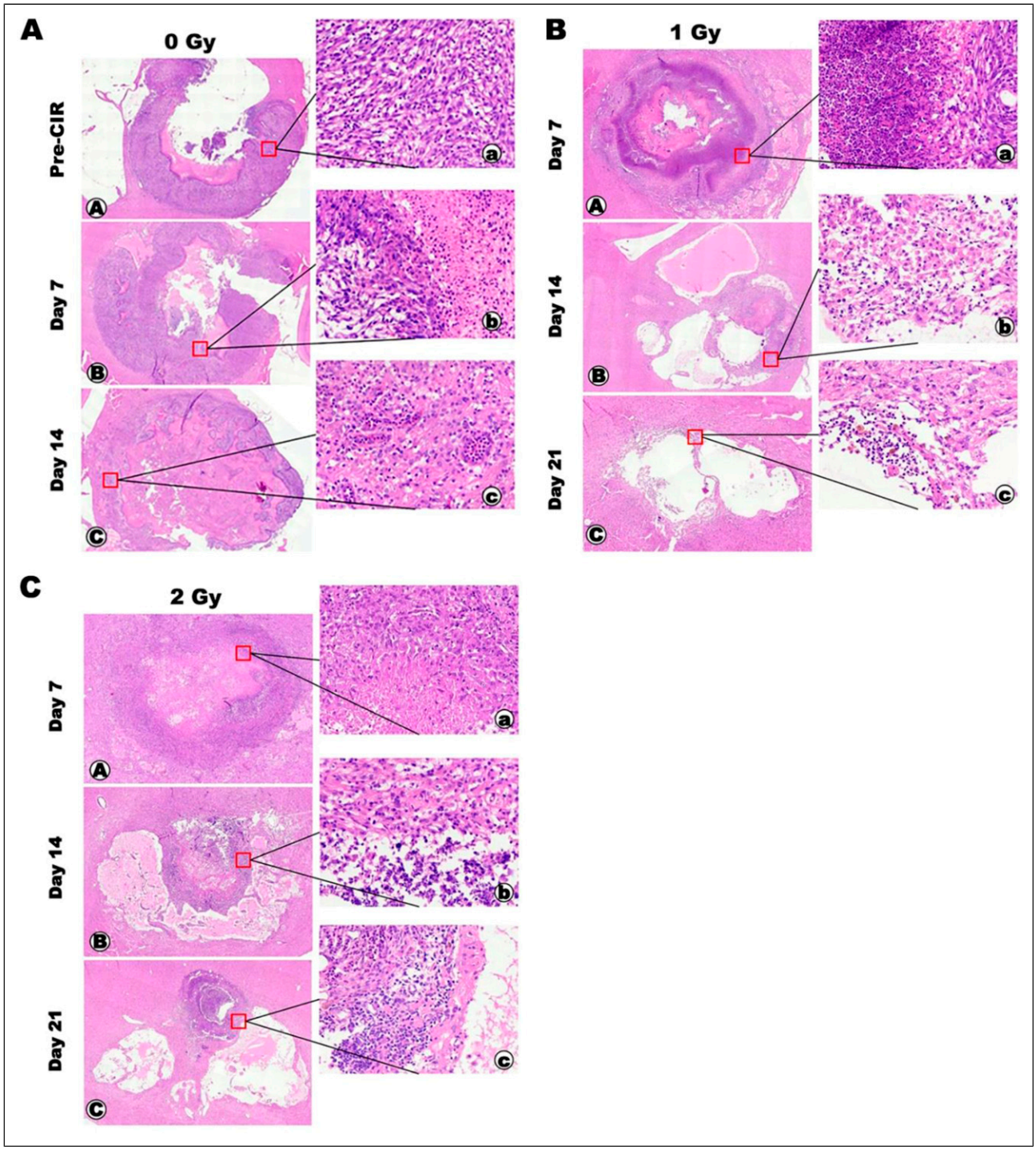

Figure 4. HE staining results of tumor tissues at multiple time points pre-CIR and post-CIR at different doses. (A-C): ×20, (a-c): ×200. Pre-CIR, HE staining at low magnification revealed tightly arranged tumor cells with powdery-stained, liquid, necrotic tissue at the tumor's center. Under high magnification, the tumor cells exhibited irregular morphology with large nuclei, marked heterogeneity, and active nuclear schizophrenia. Post-CIR (1 and 2 Gy), the tumor cells displayed significant necrosis, and parts of the tumor were replaced by areas of liquefaction.

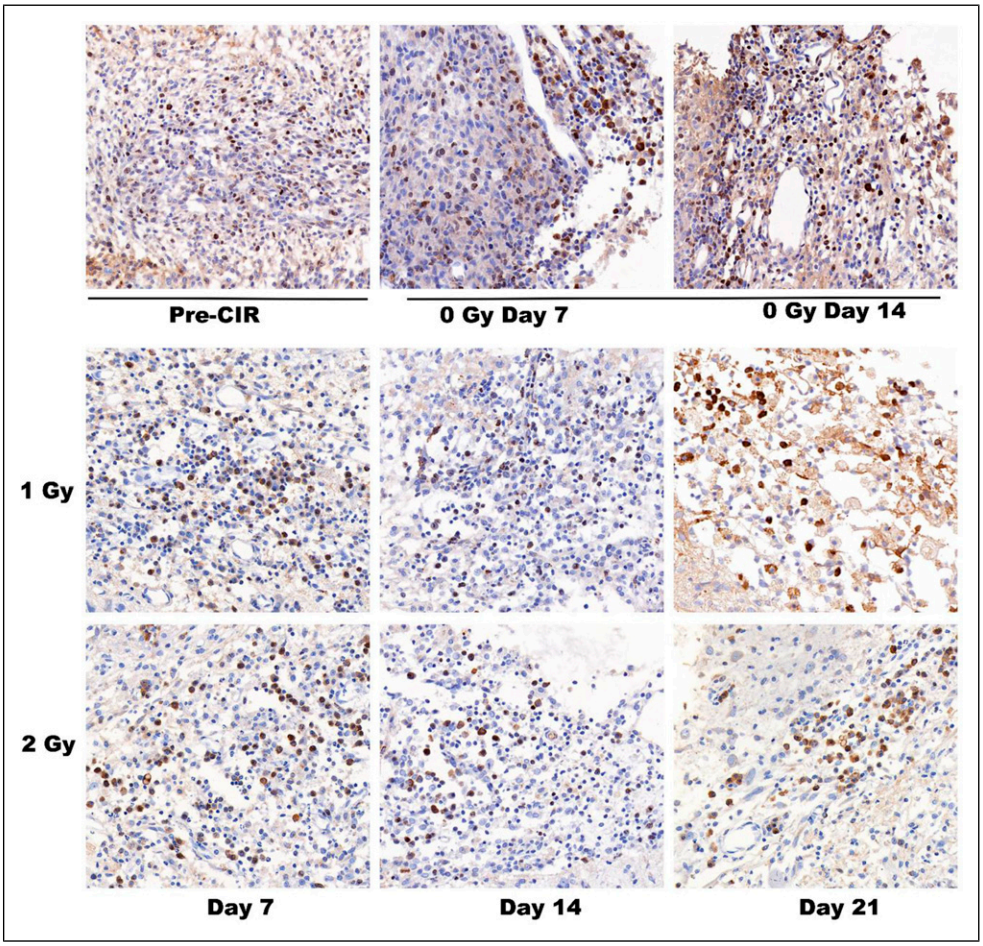

Figure 5. Ki-67 immunohistochemical staining results of tumor tissues at multiple time points pre- and post-CIR at different doses; ×200. Post-CIR (1 and 2 Gy), the Ki-67 value-added index of tumor tissues was significantly reduced.

the Ki-67 proliferation index indicated a recurrence and progression, leading us to believe that $CT_{65\ keV}$ and K of rat C6 gliomas detected by energy-spectrum CT correlate with the density and invasiveness of tumor cells. Mean-while, IC can respond to changes in the density of tumor microvessels and local mi-crocirculation,[36,37] consistent with our study findings. Additionally, the reduced expression of tumour vascular-related proteins and the reduction of the Ki-67 proliferation index post-CIR confirm the inhibitory effect of CIR on the proliferation of tumor cells and angiogenesis of rat C6 gliomas. These findings provide a theoretical basis for its potential application in clinical settings.

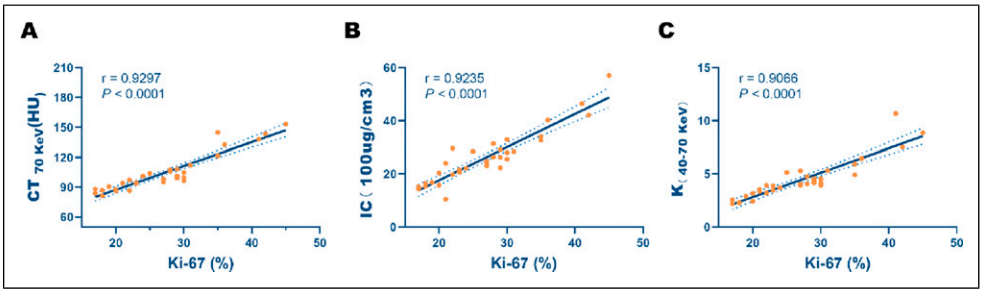

Figure 6. Correlation analysis between Ki-67 proliferation index values and energy spectrum CT measurement parameters. (A) Pearson correlation analysis of the correlation between Ki-67 proliferation index values and CT $_{70\ keV}$ (HU). (B) Pearson correlation analysis of the correlation between Ki-67 proliferation index values and iodine content (IC). (C) Pearson correlation analysis of the correlation between Ki-67 proliferation index values and the slope of the energy spectrum curve ($K_{40\text{-}70\ keV}$).

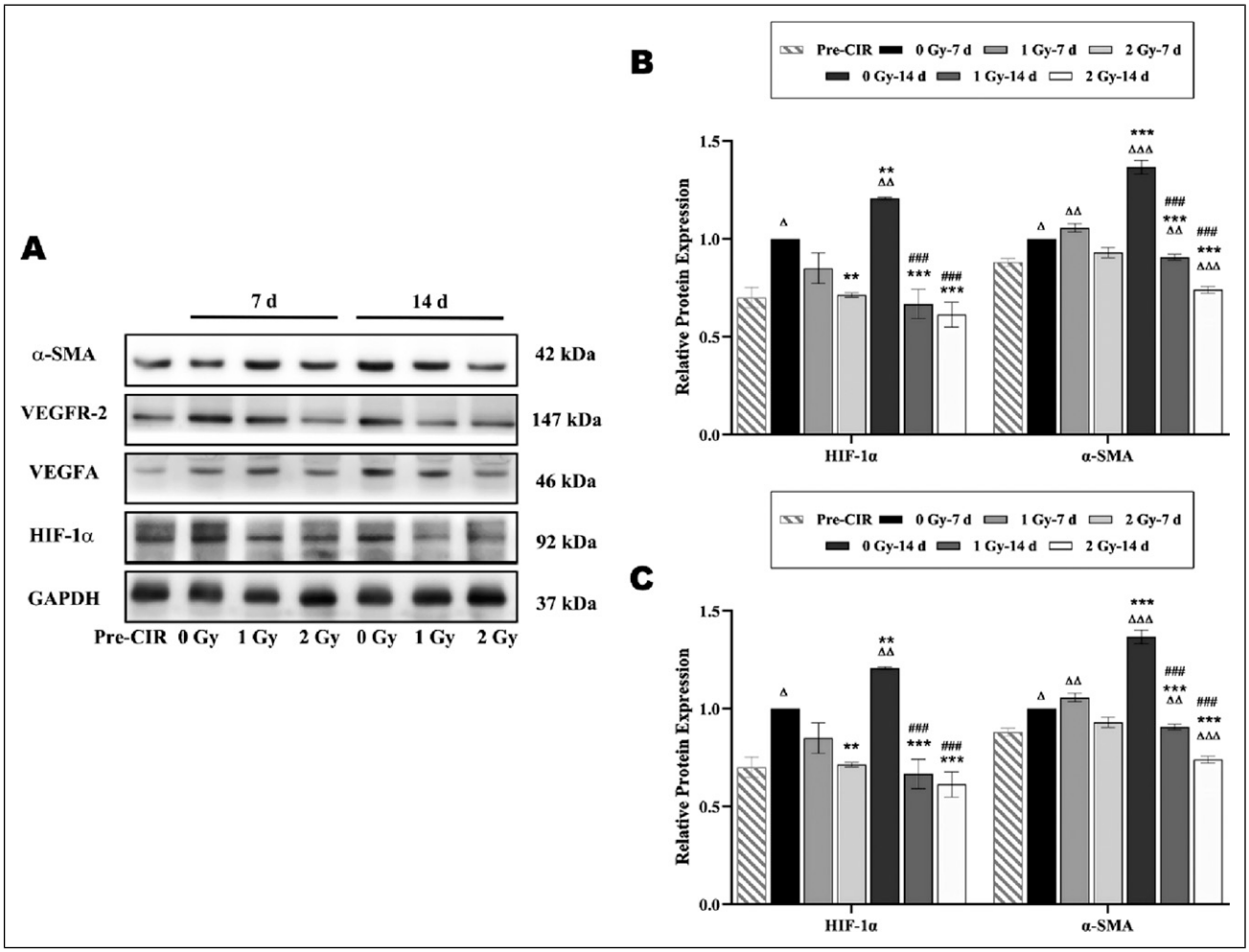

Figure 7. Changes in the expression of vascular-related proteins in tumor tissues pre- and post-CIR with different doses. (A) Vascular-related protein expression bands. (B) HIF-1a and a-SMA expression trends; (C) VEGFA and VEGFR-2 expression trends. The changes in the ex-pression of proteins were as follows: continuous up-regulation in the 0 Gy group and down-regulation in the 2 Gy group; down-regulation in the 1 Gy group on the 14th day post-CIR. The differences were statistically significant compared to pre-CIR: $^{\Delta}P < 0.05$; $^{\Delta\Delta}P < 0.01$; $^{\Delta\Delta\Delta}P < 0.001$. Moreover, the differences were statistically significant compared to 0 Gy–7d: $P < 0.05$, $^{*}P < 0.01$, $^{***}P < 0.001$; and compared to those 7 days post-CIR with the same dose: $^{\#}P < 0.05$, $^{\#\#}P < 0.01$, $^{\#\#\#}P < 0.001$.

This study has some limitations. Firstly, it should be noted that all the control rats in the 0 Gy group died 21 days after CIR. Therefore, we were unable to compare the energy-spectrum CT data with that of the carbon ion-irradiated groups. Secondly, there are functional differences and disease resistance mechanisms between animals and humans. Further in-depth studies are required to determine the potential benefits of carbon ion therapy for brain gliomas in different species. Nevertheless, our study still contributes to the experimental basis for the clinical advancements of CIRT for brain gliomas.

Conclusion

We speculate that CIR of rat C6 gliomas can effectively kill tumor cells and inhibit tumor proliferative activity to varying degrees, with 2 Gy irradiation showing better inhibitory efficacy than 1 Gy. Quantitative detection using energy-spectrum CT, combined with immunohistochemistry, could actively support carbon ion radiotherapy in inhibiting tumor proliferation. The rat C6 glioma model can be regarded as an ideal animal model for experimental studies on radiation therapy for malignant gliomas of the brain.

Acknowledgements

We gratefully acknowledge assistance for the animal experiments from The Institute of Modern Physics (IMP) of the Chinese Academy of Sciences, and research support from GE Healthcare.

Author Contributions

YFL and JLL conceived and designed the study. YFL and LT completion of experiments. HYZ and YX collected data. YFL

prepared the manuscript. QFW and LG performed the data analysis and interpretation. YFL and JLL drafted and revised the manuscript. All authors read and approved the final manuscript.

Declaration of Conflicting Interests

The author(s) declared no potential conflicts of interest with respect to the research, authorship, and/or publication of this article.

Funding

The author(s) disclosed receipt of the following financial support for the research, authorship, and/or publication of this article: This research was funded by National Natural Science Foundation of China (grant number 81960337), the Basic Research Innovation Group Project of Gansu Province (grant number 21JR7RA432), Lanzhou University "Cuiying Postgraduate Instructor" Incubation Program (Grant number CYDSPY202003), the Science and Technology Plan Project of Chengguan district (2022SHFZ0020) and Key Laboratory of Environmental Ecology and Population Health in Northwest Minority Areas (NO. MWZD202201).

ORCID iD

Jianli Liu https://orcid.org/0000-0003-2417-3558

References

1. Schaff LR, Mellinghoff IK. Glioblastoma and other primary brain malignancies in adults: a review. *JAMA*. 2023;329(7):574-587. doi:10.1001/jama.2023.0023
2. Miller KD, Ostrom QT, Kruchko C, et al. Brain and other central nervous system tumor statistics, 2021. *CA Cancer J Clin*. 2021;71(5):381-406. doi:10.3322/caac.21693
3. Molinaro AM, Hervey-Jumper S, Morshed RA, et al. Association of maximal extent of resection of contrast-enhanced and non-contrast-enhanced tumor with survival within molecular subgroups of patients with newly diagnosed glioblastoma. *JAMA Oncol*. 2020;6(4):495-503. doi:10.1001/jamaoncol.2019.6143
4. Weller M, Van Den Bent M, Preusser M, et al. Author correction: EANO guidelines on the diagnosis and treatment of diffuse gliomas of adulthood. *Nat Rev Clin Oncol*. 2022;19(5):357-358. doi:10.1038/s41571-022-00623-3
5. Harrabi SB, Bougatf N, Mohr A, et al. Dosimetric advantages of proton therapy over conventional radiotherapy with photons in young patients and adults with low-grade glioma. *Strahlenther Onkol*. 2016;192(11):759-769. doi:10.1007/s00066-016-1005-9
6. Chiblak S, Tang Z, Lemke D, et al. Carbon irradiation overcomes glioma radioresistance by eradicating stem cells and forming an antiangiogenic and immunopermissive niche. *JCI Insight*. 2019;4(2):e123837. doi:10.1172/jci.insight.123837
7. Allen C, Her S, Jaffray DA. Radiotherapy for cancer: present and future. *Adv Drug Deliv Rev*. 2017;109:1-2. doi:10.1016/j.addr.2017.01.004
8. Durante M, Orecchia R, Loeffler JS. Charged-particle therapy in cancer: clinical uses and future perspectives. *Nat Rev Clin Oncol*. 2017;14(8):483-495. doi:10.1038/nrclinonc.2017.30
9. Rackwitz T, Debus J. Clinical applications of proton and carbon ion therapy. *Semin Oncol*. 2019;46(3):226-232. doi:10.1053/j.seminoncol.2019.07.005
10. Ando K, Kase Y. Biological characteristics of carbon-ion therapy. *Int J Radiat Biol*. 2009;85(9):715-728. doi:10.1080/09553000903072470
11. Takahashi M, Hirakawa H, Yajima H, Izumi-Nakajima N, Okayasu R, Fujimori A. Carbon ion beam is more effective to induce cell death in sphere-type A172 human glioblastoma cells compared with X-rays. *Int J Radiat Biol*. 2014;90(12):1125-1132. doi:10.3109/09553002.2014.927933
12. Valable S, Gérault AN, Lambert G, et al. Impact of hypoxia on carbon ion therapy in glioblastoma cells: modulation by LET and hypoxia-dependent genes. *Cancers*. 2020;12(8):2019. doi:10.3390/cancers12082019
13. Combs SE, Bohl J, Elsasser T, et al. Radiobiological evaluation and correlation with the local effect model (LEM) of carbon ion radiation therapy and temozolomide in glioblastoma cell lines. *Int J Radiat Biol*. 2009;85(2):126-137. doi:10.1080/09553000802641151
14. Combs SE, Zipp L, Rieken S, et al. In vitro evaluation of photon and carbon ion radiotherapy in combination with chemotherapy in glioblastoma cells. *Radiat Oncol*. 2012;7:9. doi:10.1186/1748-717x-7-9
15. Liu J, Zhou J, Li J, Zhang L, Zhang P, Liu B. Evaluation of rat C6 malignant glioma using spectral computed tomography. *Exp Ther Med*. 2012;14(2):1037-1044. doi:10.3892/etm.2017.4613
16. Hong X, Liu L, Wang M, et al. Quantitative multiparametric MRI assessment of glioma response to radiotherapy in a rat model. *Neuro Oncol*. 2014;16(6):856-867. doi:10.1093/neuonc/not245
17. Meissner JE, Korzowski A, Regnery S, et al. Early response assessment of glioma patients to definitive chemoradiotherapy using chemical exchange saturation transfer imaging at 7 T. *J Magn Reson Imaging*. 2019;50(4):1268-1277. doi:10.1002/jmri.26702
18. Yeung TP, Kurdi M, Wang Y, et al. CT perfusion imaging as an early biomarker of differential response to stereotactic radiosurgery in C6 rat gliomas. *PLoS One*. 2014;9(10):e109781. doi:10.1371/journal.pone.0109781
19. Mccollough CH, Leng S, Yu L, Fletcher JG. Dual- and multi-energy CT: principles, technical approaches, and clinical applications. *Radiology*. 2015;276(3):637-653. doi:10.1148/radiol.2015142631
20. Biau J, Chautard E, De Koning L, et al. Predictive biomarkers of resistance to hypofractionated radiotherapy in high grade glioma. *Radiat Oncol*. 2017;12(1):123. doi:10.1186/s13014-017-0858-0
21. Liermann J, Shinoto M, Syed M, Debus J, Herfarth K, Naumann P. Carbon ion radiotherapy in pancreatic cancer: a review of clinical data. *Radiother Oncol*. 2020;147:145-150. doi:10.1016/j.radonc.2020.05.012
22. Keta OD, Todorović DV, Bulat TM, et al. Comparison of human lung cancer cell radiosensitivity after irradiations with

therapeutic protons and carbon ions. *Exp Biol Med*. 2017; 242(10):1015-1024. doi:10.1177/1535370216669611

23. Sai S, Vares G, Kim EH, et al. Carbon ion beam combined with cisplatin effectively disrupts triple negative breast cancer stem-like cells in vitro. *Mol Cancer*. 2015;14:166. doi:10.1186/s12943-015-0429-7
24. Kong L, Gao J, Hu J, et al. Carbon ion radiotherapy boost in the treatment of glioblastoma: a randomized phase I/III clinical trial. *Cancer*. 2019;39(1):5. doi:10.1186/s40880-019-0351-2
25. Combs SE, Kieser M, Rieken S, et al. Randomized phase II study evaluating a carbon ion boost applied after combined radiochemotherapy with temozolomide versus a proton boost after radiochemotherapy with temozolomide in patients with primary glioblastoma: the CLEOPATRA trial. *BMC Cancer*. 2010;10:478. doi:10.1186/1471-2407-10-478
26. Combs SE, Burkholder I, Edler L, et al. Randomised phase I/II study to evaluate carbon ion radiotherapy versus fractionated stereotactic radiotherapy in patients with recurrent or progressive gliomas: the CINDERELLA trial. *BMC Cancer*. 2010;10:533. doi:10.1186/1471-2407-10-533
27. Lautenschlaeger FS, Dumke R, Schymalla M, et al. Comparison of carbon ion and photon reirradiation for recurrent glioblastoma. *Strahlenther Onkol*. 2022;198(5):427-435. doi:10.1007/s00066-021-01844-8
28. Huang W, Li J, Geng X, et al. The reactive astrocytes after surgical brain injury potentiates the migration, invasion, and angiogenesis of C6 glioma. *World Neurosurg*. 2022;168:e595-e606. doi:10.1016/j.wneu.2022.10.064
29. Park JM, Kim JI, Wu HG. Technological advances in charged-particle therapy. *Cancer Res Treat*. 2021;53(3):635-640. doi:10.4143/crt.2021.706
30. Combs SE, Ellerbrock M, Haberer T, et al. Heidelberg ion therapy center (HIT): initial clinical experience in the first 80 patients. *Acta Oncol*. 2010;49(7):1132-1140. doi:10.3109/0284186x.2010.498432
31. Rieken S, Habermehl D, Nikoghosyan A, et al. Assessment of early toxicity and response in patients treated with proton and carbon ion therapy at the Heidelberg ion therapy center using the raster scanning technique. *Int J Radiat Oncol Biol Phys*. 2011;81(5):e793-801. doi:10.1016/j.ijrobp.2010.12.018
32. Oishi T, Sasaki A, Hamada N, et al. Proliferation and cell death of human glioblastoma cells after carbon-ion beam exposure: morphologic and morphometric analyses. *Neuropathology*. 2008;28(4):408-416. doi:10.1111/j.1440-1789.2008.00899.x
33. Jin X, Li F, Zheng X, et al. Carbon ions induce autophagy effectively through stimulating the unfolded protein response and subsequent inhibiting Akt phosphorylation in tumor cells. *Sci Rep*. 2015;5:13815. doi:10.1038/srep13815
34. Yingying L, Zhe Z, Xiaochen W, Xiaomei L, Nan J, Shengjun S. Dual-layer detector spectral CT-a new supplementary method for preoperative evaluation of glioma. *Eur J Radiol*. 2021;138:109649. doi:10.1016/j.ejrad.2021.109649
35. Han L, Huang X, Liu X, et al. Evaluation of the anti-angiogenic effect of bevacizumab on rat C6 glioma by spectral computed tomography. *Acta Radiol*. 2021;62(1):120-128. doi:10.1177/0284185120916200
36. Huang X, Liang X, Zhang Q, et al. Quantifying the angiogenesis of C6 glioma in rats based on CT quantitative parameters. *Acta Radiol*. 2019;60(8):985-993. doi:10.1177/0284185118808073
37. Lv Y, Zhou J, Lv X, et al. Dual-energy spectral CT quantitative parameters for the differentiation of Glioma recurrence from treatment-related changes: a preliminary study. *BMC Med Imaging*. 2020;20(1):5. doi:10.1186/s12880-019-0406-5